ANNALI DI GEOFISICA, VOL. XXXVII, N. 6, December 1994

The effect of lateral variations of friction on crustal faulting

John Boatwright([1]) **and Massimo Cocco**([2])
([1]) *U.S. Geological Survey, Menlo Park, CA, U.S.A.*
([2]) *Istituto Nazionale di Geofisica, Roma, Italy*

Abstract
We propose that lateral variations in fault friction control the heterogeneity of slip observed in large earthquakes. We model these variations using a rate and state-dependent friction law, where we differentiate velocity-weakening into strong and weak-seismic fields, and velocity-strengthening into compliant and viscous fields. The strong-seismic field comprises the seismic slip concentrations, or asperities. The two «intermediate» frictional fields, weak-seismic and compliant, modulate both the tectonic loading and the dynamic rupture process. During the interseismic period, the compliant and viscous regions slip aseismically while the strong-seismic regions remain locked, evolving into stress concentrations that fail only in main shocks. The weak-seismic regions contain most of the interseismic activity and aftershocks, but also «creep seismically», that is, most of the weak-seismic area slips aseismically, actuating the seismicity on the remaining area. This «mixed» frictional behavior can be obtained from a sufficiently heterogenous distribution for the critical slip distance. The interseismic slip provides an inherent rupture resistance: dynamic rupture fronts decelerate as they penetrate into these unloaded compliant or creeping weak-seismic areas, diffusing into broad areas of accelerated afterslip. Aftershocks occur in both the weak-seismic and compliant areas around the fault, but most of the stress is diffused through aseismic slip. Rapid afterslip on these peripheral areas can also produce aftershocks within the main shock rupture area, by reloading weak fault areas that slipped in the main shock and then healed. We test this frictional model by comparing the interevent seismicity and aftershocks to the coseismic slip distribution for the 1966 Parkfield, 1979 Coyote Lake, and 1984 Morgan Hill earthquakes.

Key words *friction – faulting – aftershocks – aseismic slip*

1. Introduction

Frictional models of crustal faults have been widely adopted to describe the mechanics of crustal faulting. The variation of frictional resistance during sliding can yield a dynamic instability that results in a sudden slip associated with a stress drop. The frictional behavior in which friction has a negative dependence on sliding velocity is known as velocity weakening (Ruina, 1980, 1983; Rice and Gu, 1983; Gu *et al.*, 1984; Dieterich, 1978, 1979a). Because the strength parameters are time dependent (Dieterich, 1978), velocity weakening frictional models provide a mechanism by which strength is regained after the instability (Scholz, 1989). Stability analyses show that the behavior of friction depends on the material properties, and load conditions. Under specified load conditions, the faulting episodes are characterized by the alternation of velocity strengthening and velocity weakening fields that control stable and unstable slip on the fault.

Tse and Rice (1986) discuss the behavior of strain release on vertical strike-slip faults in order to demonstrate how the depth dependence of friction influences the phenomenology of crustal faulting. In particular, they show how progressive slip on the aseismic, velocity-strengthening, section of the fault at depth con-

centrates stress on the seismic, velocity-weakening, section of the fault in the mid-crust. When the dynamic failure of the seismic mid-crust occurs, slip can penetrate into the aseismic section of the fault. Tse and Rice (1986) demonstrate that the postseismic slip on the deep sections of the fault gradually devolves to the steady interseismic slip.

Scholz (1989) discusses the depth variations of frictional behaviors and fault-zone rheology in order to identify the stability transitions at different depths. Scholz (1989) points out that stable and unstable slip occurs within the brittle rheological field, and that stability transitions occur at shallower depths than the brittle/ductile rheological transition. These studies clearly show that, although the behavior of the velocity-weakening section of the mid-crust determines the characteristics of the earthquake cycle, the interaction between the velocity-weakening and velocity-strengthening sections of the fault strongly conditions the general character of the faulting process.

In this paper, we discuss the observations of the spatial distribution of slip (or seismic moment), the distribution of aftershock hypocenters on the fault plane, and the spatial and temporal evolution of afterslip in order to propose that lateral variations in friction are similarly significant, even if less pronounced, than the vertical variations discussed by Tse and Rice (1986) and Scholz (1989). In particular, we suggest that variations between velocity-strengthening and velocity-weakening sections, along the strike direction of the fault, control the source complexity. This model explains the heterogeneous seismic moment release commonly observed in large earthquakes, and the concentrations of slip (and stress) which have been described as «asperities» following Kanamori (1981). Explicitly, these asperities represent velocity-weakening regions that have been loaded both by the ongoing slip at depth and by the interseismic slip on the surrounding velocity-strengthening areas of the fault zone.

The general assumptions of our model have been discussed by several authors, in particular, by Tse *et al.* (1985), in a model of geodetic observations at Parkfield, and by Scholz (1989) in a conceptual model for the seismic coupling of subduction zones. However, in this paper we discuss some common aspects of vertical strike-slip faulting episodes, such as the general co-location of interseismic earthquakes and aftershocks, and the distribution of coseismic slip to suggest that the velocity-weakening or seismic regions can be reasonably subdivided into strong and weak-seismic areas. Strong-seismic areas are those sections of the fault that exhibit almost no interseismic events or foreshocks, few aftershocks, and where coseismic slip is concentrated. In contrast, weak-seismic areas exhibit interseismic activity, foreshocks, aftershocks, and deficits of coseismic slip. Contiguous strong and weak-seismic areas may fail together in main shocks, but the weak-seismic areas have smaller stress drops and less slip than the strong-seismic areas. Because their frictional characteristics are intermediate to those of the strong-seismic and the velocity-strengthening areas, weak-seismic areas are often interposed between these other areas.

Dieterich (1986) suggests that instabilities can occur within the velocity strengthening field under particular values of frictional parameters and load conditions. We have verified his supposition using a dynamic spring slider model. Noting this result, we propose that velocity-strengthening behavior be subdivided between compliant and viscous behavior. A compliant area is a velocity-strengthening region of the fault that, under appropriate load conditions, can sustain an instability. On the contrary, viscous areas are those sections of the fault that only slip aseismically.

The evidence for the widespread occurrence of velocity-strengthening regions in the mid and upper crust is required by observations of surficial afterslip following moderate strike-slip earthquakes (Marone *et al.*, 1991), and more critically, this behavior is required at many of the rupture boundaries inferred for large earthquakes. If coseismic rupture terminates at geometrical complexities of the fault, such as bends or steps (Sibson, 1986; Scholz, 1990), we generally observe that seismicity clusters at rupture boundaries. However, the seismicity of strike-slip fault zones indicates that the fault segments, without geometrical

complexities at their ends, are often bounded by areas which exhibit no aftershocks. Because these boundaries are strongly loaded by the stress redistribution of the main shock, they would exhibit aftershocks if they were seismic or velocity-weakening. Thus, we infer that these rupture boundaries are aseismic and velocity-strengthening, and further, that this velocity-strengthening behavior contributed to the arrest of the dynamic rupture. Such aseismic areas have been described previously as «absorbing barriers» by Aki (1978) and King (1986).

2. Rate and state-variable friction laws

In order to define the range of frictional behaviors that together constitute the phenomena of crustal faulting, we need briefly to discuss the rate- and state-variable constitutive laws. The frictional characteristics for the crustal faulting process that are considered in this paper are entirely contained within the rheological framework both discerned in the laboratory and parameterized by Dieterich (1978, 1979a,b, 1980, 1981, 1986). Owing to its relatively simple form, we use the state-variable description derived by Ruina (1980, 1983), which has been discussed in detail by many authors, in particular, by Rice and Gu (1983), Gu *et al.* (1984), and Tse and Rice (1986).

The description of the behavior of frictional sliding surfaces proposed by Ruina (1980, 1983) is based on two coupled equations. The first equation relates the traction τ necessary to slide the surface to the state variable θ and the sliding velocity V:

$$\tau = \tau_* + \theta + A \ln (V/V_*) . \qquad (2.1)$$

Here τ_* and V_* are a reference traction and sliding velocity: τ_* is the traction required to steadily slide the surface at the velocity V_*. The state variable θ provides a memory for the sliding surface: for a system which is being loaded at a constant rate but is moving at a very slow velocity, θ increases proportionally with the time since the last instability (Dieterich, 1986). We refer to eq. (2.1) as the *governing* equation. The time evolution of the state variable is described by the second equation

$$\frac{d\theta}{dt} = -\frac{V}{L}\left(\theta + B \ln (V/V_*)\right) . \qquad (2.2)$$

Here L is the *critical slip distance* over which the surface slips before the motion approximates steady-state sliding. A and B are positive constants that depend on the material properties, temperature, and pressure. We refer to eq. (2.2) as the *evolution* equation. The governing eq. (2.1) assumes that the sliding surface is always in motion, although possibly sliding more slowly than can be measured.

In the steady-state limit, that is $d\theta / dt = 0$, the state variable is constant over time and the evolution equation is reduced to

$$\theta_{ss} (V) = -B \ln (V / V_*) . \qquad (2.3a)$$

Substituting the relation for θ_{ss} into the governing equation yields an equation for the steady-state traction,

$$\tau_{ss} (V) = \tau_* - (B - A) \ln (V / V_*) . \qquad (2.3b)$$

The evolution of the state variable is generally self-damping: the further the system is from the steady-state, the more rapidly the state variable evolves towards the steady-state solution.

Figure 1 shows the behavior of traction and sliding velocity versus slip, for an experiment of frictional sliding where a unitary surface is forced to slide at constant velocities. When the sliding velocity is changed, there is an abrupt change in the traction, after which the traction decays towards a new steady-state value as the surface is displaced by the critical slip distance L. The traction change is $\Delta\tau = (B - A) \ln (V_1 / V_0)$, where V_0 is the initial sliding velocity and V_1 is the new sliding velocity resulting from eqs. (2.3a) and (2.3b). For the experiment depicted in fig. 1, $B > A$ and the steady-state traction decreases with increasing sliding velocity so that the surface is velocity weakening.

The quantity $(B - A)$ thus determines the sign of $d\tau_{ss} / dV$; Rice and Ruina (1983), Gu

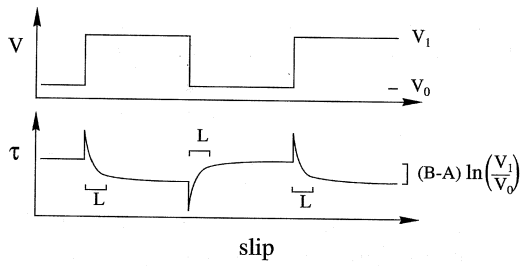

Fig. 1. Behavior of traction and sliding velocity as a function of slip in a frictional sliding experiment, where a surface is forced to slide at constant velocity and the traction required to slide the surface is monitored. When the sliding velocity suddenly changes from V_0 to V_1, there is an abrupt change in traction $\Delta\tau = A \ln (V_1 / V_0)$, after which the traction decays towards a new steady state value as the surface slips the critical slip distance L.

et al. (1984) have conducted stability analyses of the system of eqs. (2.1) and (2.2) which indicate that for $d\tau_{ss} / dV > 0$, the sliding is stable and the surface is aseismic, while for $d\tau_{ss} / dV < 0$, the sliding is unstable and the surface is possibly seismic, that is, under appropriate loading conditions the slip can accelerate to instability and some of the stored elastic energy is radiated seismically. This implies that the velocity weakening and the velocity strengthening fields are characterized by the sign of the quantity $B - A$: if $B - A > 0$, the sliding is velocity weakening, while if $B - A < 0$, it is velocity strengthening. Moreover, we note that the constants A and B introduced in eqs. (2.1) and (2.2) generally depend on the normal stress σ_n as

$$A = a\sigma_n \qquad B = b\sigma_n$$

where a and b depend on temperature, stress, and material properties. Thus, the depth variation of A and B is determined by the depth variation of the temperature and the normal stress.

To demonstrate the range of frictional behaviors that constitute the crustal faulting process, it is convenient to study the motion of a spring slider system. This system can be represented as a rigid block or slider loaded by a linear spring whose end is constrained either with a given load point traction τ_0 or a given load point velocity V_0. The equation of motion of the system is

$$m\frac{d^2\delta}{dt^2} = \tau_0 - k\delta - \tau \qquad (2.4)$$

where m is the mass of the slider, δ is the slip, k is the spring constant or stiffness, $k\delta$ is the spring force, and τ is the resistive traction, that is, the friction. Setting the forcing traction equal to the sliding resistance yields the equation of motion for the spring slider

$$\left(\frac{T}{2\pi}\right)^2 \frac{d^2\delta}{dt^2} = \frac{1}{k}(\tau_0 - \tau) - \delta \qquad (2.5)$$

where δ is the displacement of the sliding surface and $T / 2\pi$ is a characteristic vibrational or inertial time (Rice and Tse, 1986).

Rice and Tse (1986) discuss the prohibitive difficulties that arise when one attempts to solve the complete set of equations, that is, eq. (2.5) combined with the appropriate constitutive laws (eqs. (2.1) and (2.2)), throughout the entire cycle of the spring slider. If the slider motion is quasi-static, however, then

$$\frac{d^2\delta}{dt^2} \approx 0$$

and the complexity of the solution is significantly reduced. The quasi-static equation of motion is obtained by setting $T = 0$ in eq. (2.5).

Dieterich (1978 and 1979a) observed that the steady-state traction τ_{ss} becomes independent of V at sliding velocities greater than $V_c \approx 0.1$ mm/s. For $V \geq V_c$ eq. (2.3b) becomes

$$\tau_{ss} = \tau_* - (B - A) \ln (V_c / V_*). \qquad (2.6)$$

Rice and Tse (1986) and Tse and Rice (1986) combine eqs. (2.3b) and (2.6) into a single algebraic form for the steady-state traction. We have used V_c as the limit between the quasi-

static and dynamic solutions of the spring slider equation of motion, similarly to the velocity above which the steady-state friction becomes independent of the velocity (Dieterich, 1978). The equation of motion for the spring slider is then solved quasi-statically at low sliding velocities and dynamically for high sliding velocities by using eq. (2.5). In this way, the equations of motion and the constitutive relations share the same limits, greatly simplifying the programming required to solve for the behavior of the spring slider. The equation of motion is solved by integrating the resulting system of ordinary differential equation numerically using the Runge-Kutta method (Press *et al.*, 1979). Okubo and Dieterich (1986) and Okubo (1989), compared dynamic slip predictions obtained by using the constitutive law stated by eq. (2.1) and those obtained by using eq. (2.6). They found that the constitutive relation (2.6), in which the velocity effect becomes neutral at high velocity, provides better estimates of the dynamic stress drop than those obtained using eq. (2.1).

Quasi-static analyses (Rice and Ruina, 1983; Gu *et al.*, 1984) have demonstrated that for $B > A$, this system can accelerate to instability only if the spring stiffness k is less than the critical stiffness k_{cr}:

$$\frac{\Delta\tau}{\delta} = k < k_{cr} = \frac{B-A}{L} . \qquad (2.7)$$

Here $\Delta\tau$ is the stress drop corresponding to the slip δ. Equation (2.7) provides a definition of the stiffness as the ratio $\Delta\tau/\delta$ (Dieterich, 1978). If the system is stiffer than the critical stiffness, then it cannot accelerate into an instability under a steadily applied load, although it can behave unstably for more abrupt loads. Scholz (1989) uses this limit to define a *conditionally stable* frictional behavior intermediate to the *unstable* velocity-weakening field and the *stable* velocity-strengthening field.

It is important to point out that for actual faults, the stiffness k is determined by the faulting process itself (that is, $k = \Delta\sigma/\delta \propto 1/r$ where r is the length of the crack), so that the parametric boundary $k = k_{cr}$ depends on the size of the earthquake. Dieterich (1986) combines the relation for the critical stiffness (2.7) with a relation for patch stiffness

$$k = \frac{\Delta\tau}{\delta} = \frac{\eta\mu}{r}$$

in which μ is the rigidity, η is a geometrical constant which is slightly less than 1 for a circular fault, and r is the crack radius. This manipulation yields a minimum crack radius for unstable fault slip

$$r_c > \frac{\eta\mu L}{B-A} . \qquad (2.8)$$

Although it represents a relatively weak constraint, we can use eq. (2.8) to consider bounds on L for seismic regions of the crust for which there are estimates or observations of the minimum source radius.

3. Variation of frictional properties with depth

Tse and Rice (1986) discuss the behavior of A/σ_n and $(B-A)/\sigma_n$ as a function of temperature. They combine results from laboratory analyses of the frictional characteristics of Westerly granite with the central San Andreas fault geotherm derived by Lachenbruch and Sass (1973) to obtain two slightly different estimates for the behavior of A and B as a function of depth. Under the assumption that the effective normal stress varies as $\sigma_n(z) = 180\,z + 100$ bars, Tse and Rice (1986) shows that $B(z)$ linearly increases (and it exceeds $A(z)$ by a constant fraction) until depths of $z = 8\frac{1}{2}$ and $6\frac{1}{2}$ km, respectively. Below these depths, $A(z)$ continues to increase linearly with depth while $B(z)$ decreases until $z \approx 18$ km, where $B(z) = 0$ and $A(z)$ increases more strongly with depth. These two estimates are replotted in fig. 2.

Because the estimates of $A(z)$ and $B(z)$ reported by Tse and Rice (1986) (fig. 2) are obtained for a single rock-type under simplifying assumptions for the variation of temperature

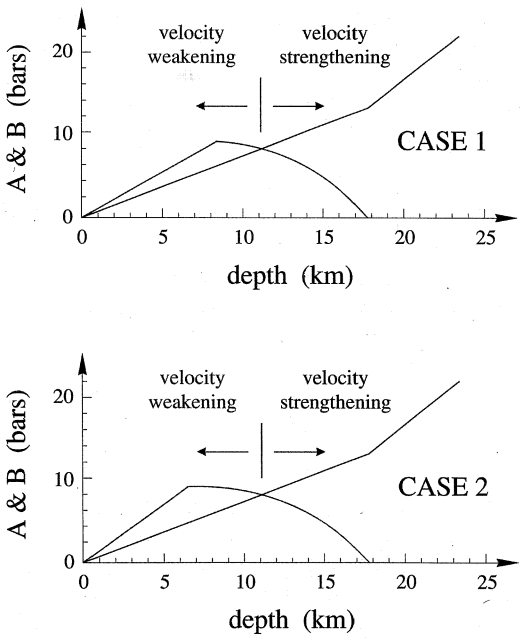

Fig. 2. Behavior of A and B as a function of depth, redrawn from Tse and Rice (1986). Case 1 and Case 2 differ for the behavior of $B(z)$ that linearly increases up to a depth of 8.5 km (Case 1), and up to a depth of 6.5 km (Case 2). Below these depths, $B(z)$ decreases to zero at $z = 18$ km for both cases. For $0 < z < 11$ km $B > A$, and the frictional response is velocity-weakening; below $z = 11$ km $B < A$ and the frictional field is velocity-strengthening.

and effective normal stress with depth, we consider them indicative of the possible range of behavior of $A(z)$ and $B(z)$ rather than characteristic of $A(z)$ and $B(z)$ everywhere along the central San Andreas. In particular, recent analyses of the behavior of faults with gouge by Marone *et al.* (1990) suggest that $A > B$ for gouge under low normal stress, so that the near-surface sections of crustal faults are velocity-strengthening. Similarly, we expect that there are extended regions at depth where $B(z) \approx A(z)$ and which behave either as weak-seismic areas or compliant areas, depending on the parameters A, B, and L. The relatively abrupt transition from velocity-weakening to velocity-strengthening that occurs at $z = 11$ km in Tse and Rice (1986) represents only one realization of the depth-dependence of these parameters.

4. Four fields of frictional behavior

Our interpretative model is obtained by dividing the range of possible frictional behaviors into four different fields: strong-seismic, weak-seismic, compliant, and viscous. This division is motivated more by the phenomenological differences between these fields than by explicit limits for the parameters A, B, and L. Note that the frictional behavior of these sliders varies continuously across the boundary $A = B$ that separates the velocity-weakening field from the velocity-strengthening field. Although the boundary $k = k_{cr}$ limits the spring slider response from seismic to aseismic under conditions of gradual loading, we demonstrate that the behavior of sliders near this parametric boundary are similar under abrupt loading.

Table I shows a synoptic description of the four fields of frictional behavior. In order to discuss these behaviors, we indicate possible ranges for the parameters A, B, and L. The stress release during failure (or the dynamic stress drop) and the relative strength, and consequently the recurrence time for failure, are determined by $B - A$ and A, respectively (Mikumo, 1992). We make the broad assumption that L is distributed heterogeneously over a fault zone, while A and B vary more slowly through their dependence on normal stress, temperature and lithology. Such a distribution for L represents one of the parameter descriptions proposed and discussed by Dieterich (1986). If L were uniform on crustal faults, then the minimum source radius should be fixed within areas where $(B - A)$ is approximately constant. Because this lower limit of earthquake size is not observed, that is, the frequency-magnitude statistics of earthquakes do not change at small magnitudes, then L must be distributed heterogeneously on real faults.

This stochastic interpretation corresponds with the wide range for L used in recent analysis of the behavior of crustal faults. Dieterich (1986) favors $L \approx 10$ μm values, derived from

Table I. Four fields of frictional parameters.

Description	$A\&B$	L	Seismicity	Strain release
Strong (seismic)	$B > A$	1-10 mm ?	Main shocks and few aftershocks	Episodic dynamic slip
Weak (seismic)	$B > A$ $B - A \leq \varepsilon$	10μm - 1 mm ?	Interevent seismicity, foreshocks, and aftershocks	Dynamic slip and creep
Compliant (conditionally seismic)	$B < A$ $A - B \leq$A ε	mm - cm ?	Early aftershocks	Creep and forced slip
Viscous (aseismic)	$A \gg B$	cm ?	None	Stable sliding

laboratory analyses, in his models of crustal rupture nucleation. Scholz (1988) proposes that at seismogenic depths L is in the range 1 to 10 mm. Similar values are assumed by Tse and Rice (1986) who show that for L greater than 10 cm the fault behavior is entirely stable. Miyatake (1992) assumes that L increases at high slip rates, and he proposes a modified version of rate- and state-dependent friction law with a rate-dependent law for L. This range of assumed behavior suggests that L might reasonably vary from 1 μ m $\leq L \leq$ 1 cm on crustal fault zones. We consider the consequences of this stochastic assumption for L as we discuss the frictional behavior inferred for crustal fault zones.

Strong-seismic – Strong-seismic areas are velocity-weakening fault sections where large stress drops and relatively large slips occur, driving the rupture process of large earthquakes. These areas were described as asperities by Kanamori (1981): we use strong-seismic to avoid confusion with the use of asperity in fracture mechanics, where asperities are the isolated areas of contact on a fault surface. On strong-seismic areas $B - A$ is positive; the greater $B - A$, the stronger the frictional response of the fault area. Observationally, these strong seismic areas exhibit little interseismic activity and few aftershocks. In general, strong-seismic areas do not creep during the interseismic period: if the distribution for L has a sufficiently long tail, however, there can be localized areas with interseismic creep.

It is difficult to estimate the critical slip distance L from observations of strong-seismic areas. Tse and Rice (1986) assume $5 \leq L \leq 40$ mm, using L's that are constant throughout the crust, but their lower limit is predicated on stability and CPU considerations. The possibility of estimating L for these regions from the minimum earthquake size is vitiated by the fact that few aftershocks or interseismic earthquakes are located in strong-seismic areas. As an example, however, if the minimum magnitude for earthquakes observed in a strong-seismic region were $M \leq 2$, then the assumption of a 10 bar stress drop yields $r_c \leq 75$ m and $L \leq 1$ mm.

Weak-seismic – In contrast to strong-seismic regions, which have few small earthquakes, weak-seismic regions contain most of the microearthquakes that occur in the interseismic, preseismic, and postseismic parts of the cycle. Weak-seismic areas have positive $(B - A)$'s, but are close to the neutral limit $B \approx A$. For spring slider models, this range corresponds to stress drops and recurrence times that are significantly smaller than those for the strong-seismic sliders, for a similar load point velocity.

Figure 3 shows a comparison of spring slider behaviors with strong and weak-seismic characteristics under constant loading. The load point velocity for the simulations is 32 mm/year: this velocity is also labelled $C\&V$ to indicate that it is the steady-state velocity of the compliant and viscous sliders. For the strong-seismic slider, $B = 6.0$ bars and $A = 5.0$ bars. For the weak-seismic slider, $B = 5.2$ bars

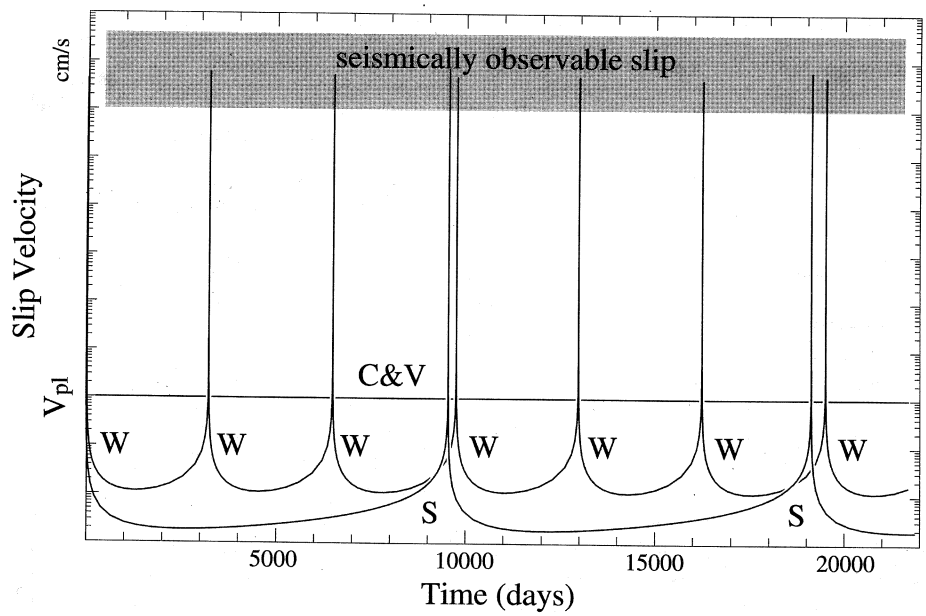

Fig. 3. Spring slider responses to a constant (tectonic) loading rate. The load velocity for this simulation is $V_0 = 32$ mm/year, $A = 5$ bar and $L = 1$ mm. The curves labelled S and W indicate the strong and the weak-seismic sliders, for which $B = 6.0$ and 5.2 bars, respectively. Their episodic behaviors illustrate the velocity-weakening response to gradual loading. The curve labelled $C\&V$ indicates the compliant and viscous sliders that slip aseismically at the load or plate velocity.

and $A = 5.0$ bars. The five-fold difference in $(B - A)$ between these sliders changes the recurrence interval by a factor of about three. The critical slip distance is assumed to be $L = 1$ mm for both sliders.

The critical slip distances for the weak-seismic field can be estimated if a minimum earthquake size can be determined. If we assume, for instance, a minimum magnitude of $M_{\min} \leq 0.5$ (this bound is representative of the observational limit for earthquakes at Parkfield-Michaels, 1991), and assume a stress drop of 5 bars, the limiting source radius is approximately 20 m. Equation (2.8) then yields a limit of $L \leq 14$ μm, if the earthquake occurs on a fault area where $(B - A) \approx 0.2$ bars. For faults systems that can be studied using borehole seismometers, it might be possible to map minimum magnitude and stress drop to evaluate the variability of L.

In weak-seismic areas where the critical slip distance exceeds $\delta(B - A)/\Delta\tau$, gradual loading produces aseismic slip. There is an inherent geometric constraint in this relation, as $\delta/\Delta\tau \propto r_p$, where r_p is the radius of the slipping patch. Scholz (1989) described this behavior as *conditionally stable*, because an event with sufficient compliance, that is, $\delta/\Delta\tau$, can produce unstable slip on the patch. The compliance of a faulting event scales with the physical extent of the earthquake.

If L is heterogeneously distributed in a weak-seismic area, then part of the fault area will slip aseismically while the rest fails in small or moderate-sized earthquakes where the stress has been concentrated by the nearby aseismic slip. If the average critical slip distance is sufficiently large, only a small fraction of the fault area will be seismic. Stress is transfered aseismically with small events seismi-

cally marking out the broader aseismic deformation (Wesson, 1987). This process of «seismic creep» appears to characterize the most seismically active areas of vertical strike-slip faults with large strain rates. The creeping section of the San Andreas fault, from Parkfield to San Juan Bautista is one example. Many earthquake swarms might also be driven by this interactive mechanism, where a broad pulse of aseismic slip loads and reloads the small earthquakes.

If a weak-seismic area is sufficiently close to a strong-seismic area that ruptures, the rupture can propagate through the weak-seismic area, albeit with less stress release and less slip than on the strong-seismic area. If the weak-seismic area is not sufficiently loaded, however, or the dynamic stress concentration not sufficiently large, the weak-seismic area will arrest the dynamic rupture. In general, if a weak-seismic area has a distribution of L which allows much of the area to slip aseismically, the area will resist dynamic rupture. In this way, weak-seismic areas can also act as the rupture «barriers» suggested by Das and Aki (1977).

Compliant – Compliant areas are velocity-strengthening fault regions that can be driven to instability if they are loaded sufficiently. The field of frictional behavior that is weakly velocity-strengthening, for which $B - A$ is negative and close to the neutral limit $B \approx A$, exhibits behavior similar to that of the weak-seismic field with $k \geq k_{cr}$. We will refer to fault areas exhibiting this frictional behavior as «compliant», noting that this behavior also falls within Scholz's (1989) phenomenological description of the *conditionally stable* field, despite $A > B$.

Figure 4 shows the response of a set of spring sliders with differing B's to an abruptly applied load of $\Delta\sigma = 13$ bars. A and L are constant and equal to 5.0 bars and 1.0 mm, respectively. The curves labelled S for strong-seismic and W for weak-seismic have B's ranging between 6.0 bars and 5.2 bars, respectively. The sliders with B's ranging between 4.8 bars and 4.0 show the compliant field, where this moderate load accelerates the slider into instabilities that occur hours after the load is applied. As B is decreased relative to A, the onset of the dynamic instability is delayed. The slider with $B = 4.0$ bars accelerates rapidly but does not reach dynamic instability.

These results demonstrate that velocity-strengthening areas can be driven to instability depending on the loading history, as Dieterich

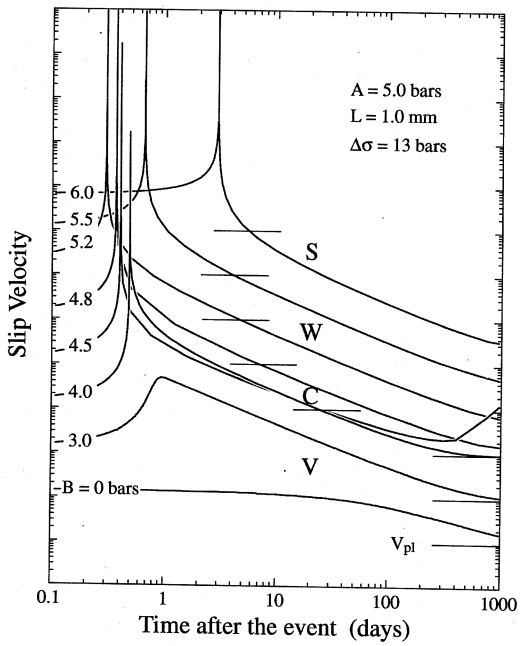

Fig. 4. Spring slider responses to an abrupt load. The load of 13 bars is applied instantaneously. For these sliders, A and L are equal to 5.0 and 1 mm, respectively. The curves labelled S and W indicate the strong and weak-seismic behavior where ($B > A$) and $B = 6.0$ and 5.2 bars, respectively. The stronger (greater $B - A$) the velocity-weakening slider, the longer the delay to instability. The curves labelled C indicate the compliant sliders with $B = 4.8$ and 4.5 bars. Note that these sliders are accelerated into instability despite their velocity-strengthening frictional characteristics. As B decreases, the acceleration of the velocity-strengthening sliders is delayed. The curves labelled V indicate the stable viscous sliders. The plate velocity is shown by the horizontal bar. Note that the curves are shifted vertically to help the comparison (the value of the plate velocity is the same for all the different curves).

(1986) suggests. This variation in response for different loading histories is the distinguishing characteristic of compliant fault areas. It is explicitly observed in the shallow sections of strike-slip faults, which exhibit prolonged afterslip following moderate-sized earthquakes such as the (M = 6.1) 1966 Parkfield and (M = 6.1) 1989 Superstition Hills events, but which rupture coseismically for larger earthquakes such as the (M = 7.3) 1991 Landers earthquake. Compliant fault areas at depth can be distinguished as those fault areas that have aftershocks but do not have interseismic activity or foreshocks.

In general, compliant areas are more resistant to dynamic failure than weak-seismic areas. This resistance derives from the increase of steady-state frictional stress $(A - B)$ ln (V/V_p) associated with an increase of slip velocity on a compliant area. Thus, as the rupture penetrates into a compliant area, the stress concentration at the rupture front weakens and the rupture decelerates. Quin (1991) used a negative stress drop as a crude model of this mechanism to arrest the updip rupture propagation in a dynamic rupture model of the 1979 Imperial Valley earthquake.

Viscous – Figure 4 shows that, as B is decreased relative to A, the instability becomes surpressed, and the frictional behavior devolves to stable sliding. This is the critical characteristic for the viscous field: the fault slides stably under either an abrupt or gradual load. In general, the response of viscous areas is relatively slow, occurring on the time frame of months and years. The gradual redistribution of stress at depth after a main shock, the so-called «visco-elastic rebound», occurs through aseismic slip on viscous areas of the fault.

We associate viscous behavior with those areas at depth below the seismogenic layer. Following Scholz (1990), the stability transition bounds the fault section where large earthquakes can nucleate, and it is different from the brittle-ductile transition that marks the maximum rupture depth for large earthquakes (Sibson, 1984). If we assume that the viscous velocity-strengthening areas are located below the zone of earthquake nucleation, then the frictional transition between compliant and viscous delimits the maximum depth of aftershocks.

In general, it is difficult to differentiate compliant and viscous areas of crustal faults. The occurrence of aftershocks is strongly conditioned by the distribution of stress release in the mainshock. Thus, there may be few compliant areas which are sufficiently stressed to drive aftershocks. For simplicity, then, in the following figures, we combine the compliant and viscous areas into a single velocity-strengthening area. In general, the shallow parts of this field may be assumed to be compliant and the deeper parts viscous.

5. The coupled asperity model

In this section, we describe a model of crustal faulting that depends on the interaction of the different frictional behaviors described in the foregoing section. Because the model incorporates many of the elements of the asperity model proposed by Kanamori (1981), but emphasizes the coupling of these asperities to the fault area surrounding them, we refer to it as the «coupled asperity» model. We focus on the different aspects of this coupling in the interseismic, coseismic, and postseismic periods.

We assume that a large earthquake is driven by the failure of one or more strong-seismic areas. Figure 5a shows a cross section of an idealized fault zone, in which the strong-seismic region is drawn arbitrarily. In general, these strong-seismic areas are surrounded by weak-seismic and compliant areas. The viscous fault areas occur at depth below the seismogenic layer. In the interseismic period, these three other frictional fields slip either continuously or episodically.

The interseismic and preseismic microseismicity is confined to the weak-seismic areas. The compliant and viscous fields creep aseismically, while the weak-seismic field creeps seismically, through a combination of seismic and aseismic slip, depending on the distributions of L and $(B - A)$. The evolving slip on nearby areas serves to increase the stress on the strong-seismic area. In turn, the presence of

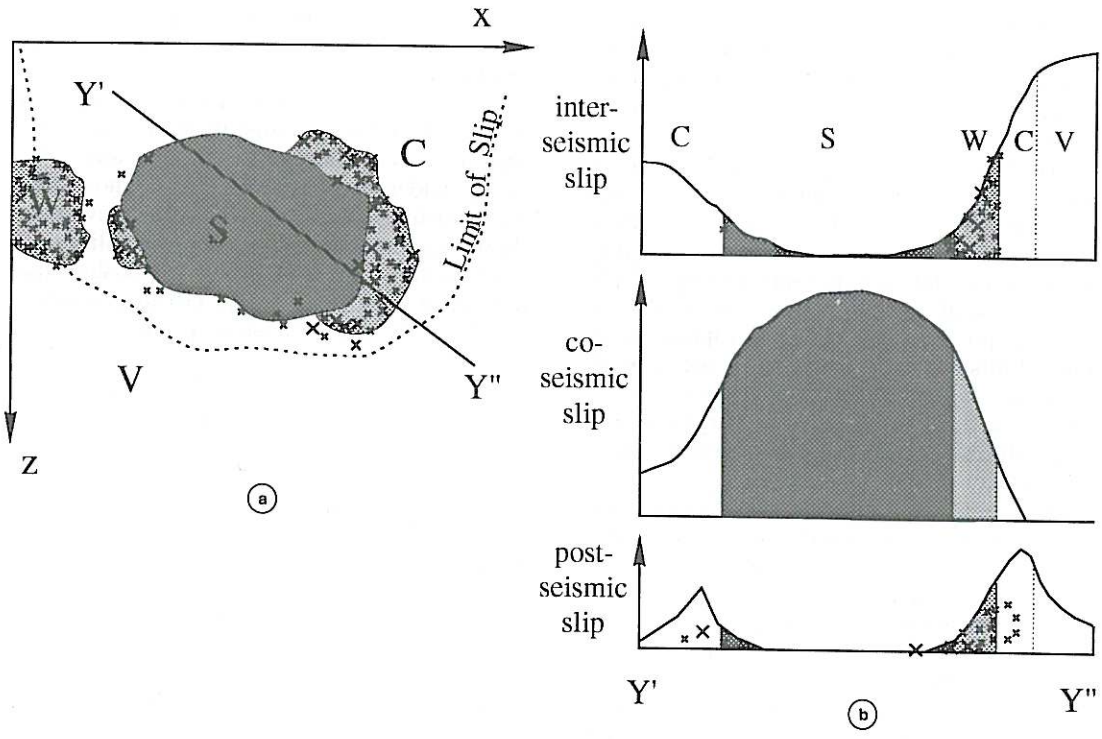

Fig. 5a,b. a) Idealized geometry of the *Coupled Asperity Model*. A single asperity (the strong-seismic area labelled S) is surrounded by weak-seismic (W) and compliant (C) areas, and lies above the viscous (V) area at depth. Crosses indicate aftershock and/or interseismic activity that occurs mostly on weak areas. When the asperity ruptures, the rupture penetrates into the surrounding weak-seismic and compliant areas. The rupture penetration shown is commensurate with a relatively large stress release on the asperity. b) An idealization of the interseismic, coseismic, and postseismic slip of the coupled asperity model, plotted along the oblique cross-section Y′-Y″.

the locked strong-seismic area retards the slip on the immediately surrounding areas, as shown in fig. 5b.

When the strong-seismic area fails in a large earthquake, the rupture extends into the weak-seismic and the compliant areas. In general, the viscous areas do not rupture dynamically. Weak-seismic areas that creep in the interseismic period can be driven to dynamic failure if the redistributed stress is sufficiently large. The stiffness of the rupture process of large earthquakes is significantly less than the stiffness characterizing the more localized slip processes in the interseismic period. Similarly, compliant areas will fail dynamically if they are sufficiently loaded.

The driving stress for the rupture of these surrounding areas is the stress redistributed by the failure of the strong-seismic areas. The further the dynamic rupture extends outside the strong-seismic area, however, the weaker the redistributed stress and the more likely the rupture arrest. As the rupture extends beyond an isolated region of stress release, the redistributed stress decreases with the inverse of the distance from the region (see for example, Das and Kostrov, 1983). At some distance outside the strong-seismic area, the stress jump is suf-

ficiently attenuated so that the dynamic rupture growth is arrested. Clearly, such an arrest can occur in either weak-seismic or compliant areas, or in a strong-seismic area that is insufficiently loaded.

The extent of rupture penetration outside the strong-seismic area is controlled by the stress level $(B - A)$ and by the size of the asperity. For a weaker faulting process, the rupture only penetrates slightly into the surrounding compliant and weak-seismic areas. For a stronger faulting process, the dynamic rupture penetrates further into the surrounding areas. Moderate ($M \approx 6$) strike-slip earthquakes cause prolonged surficial afterslip, while large ($M \approx 7$) strike-slip earthquakes rupture coseismically to the surface.

The arrest of rupture in weak-seismic and compliant areas initiates the postseismic interaction of the asperity with the surrounding fault. Figure 4 shows how compliant and viscous sliders respond to an abrupt load: the B = 4 bar slider, which does not slip dynamically, accelerates into a rapid slip event a day and a half after the load was applied. As B decreases relative to A, or as the load decreases, the slider accelerates more slowly. Figure 4 suggests that rupture arrest is an extended process in a compliant area: after the dynamic deceleration, the rupture continues to grow quasi-statically so that the rupture front diffuses into a broad zone of accelerated afterslip. Weak-seismic and compliant areas just outside the rupture area should exhibit the most immediate aftershocks and the most rapid afterslip.

The rapid afterslip that follows the arrest of dynamic rupture in compliant and weak-seismic areas is an important component of the coupled asperity model. The stress concentrations left at the edges of the dynamic rupture are diffused through aseismic slip while the weak-seismic and strong-seismic areas that ruptured in the main shock remain effectively «frozen» (Rice and Tse, 1986). The afterslip reloads the periphery of the main shock rupture area. Eventually, this reloading yields aftershocks on previously faulted areas that are seismic, but relatively weak.

In fig. 6, we plot the response of the set of spring sliders to a load with an abrupt onset that continues to grow for 30 days, tapering to a constant twice the initially applied load. This loading history is meant to represent the combination of the stress redistributed by the main shock with the stress redistributed by the afterslip, for a point outside the rupture area. The spring slider responses in fig. 6 show that weak-seismic areas which have previously slipped can sustain subsequent instabilities or aftershocks if the load grows faster than the fault heals. The large delays (10 to 200 days) of the reloaded aftershocks, result, from

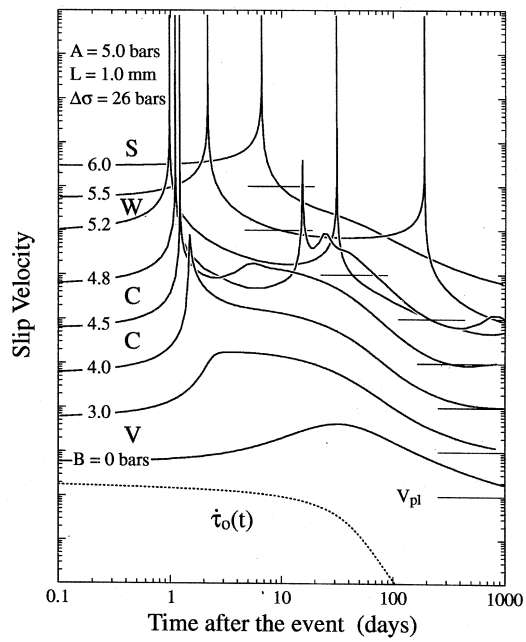

Fig. 6. Spring slider response under abrupt and continued loading. The load rate $\dot{\tau}_0$ grows for 30 days, after which it tapers to a constant value. A = 5.0 bars and L = 1 mm. The curves labelled S and W refer to the strong and weak-seismic sliders ($B > A$) for which B = 6.0 bar and B = 5.5 and 5.2 bars, respectively. The secondary instabilities for these weak sliders indicate the «reloaded» aftershocks. The weakest of the compliant sliders (that is, B = 4.8 bars) exhibits a secondary slip episode, but does not accelerate to dynamic instability. The plate velocity is shown by the horizontal bar. Note that the curves are shifted vertically to help the comparison (the value of the plate velocity is the same for all the different curves).

the delay (≈ 1 day) of the initial instabilities: if the initial load was larger, the sliders would fail more rapidly and be reloaded more rapidly.

The rapid aseismic reloading of weakly healed fault areas yields a new model for aftershocks within the main shock rupture area, alternative to the delayed failure of isolated strong fault patches. Figure 6 indicates that these reloaded aftershocks only occur within a narrow range of frictional parameters, that is, on weak-seismic areas. The reloaded aftershocks also have less slip than the initial events. Thus, reloaded aftershocks should have small stress drops, relative to the main shock. In contrast, aftershocks that represent the delayed failure of unruptured fault areas should have stress drops comparable to those of the main shock.

This reloading model for aftershocks is anticipated in Dieterich (1972), who generated aftershock sequences using a spring and block model of faulting in which the frictional strength was time-dependent and the medium had a viscoelastic or Maxwellian character. Dieterich's subsequent (1978, 1980) modelling of fault friction confirmed his assertions for the time-dependence of fault strength. The rapid afterslip on the compliant areas of the «coupled asperity» model provides the viscoelastic response required to reload the fault area.

Comparisons of aftershock locations with the slip distributions of moderate and large earthquakes by Mendoza and Hartzell (1988) appear to corroborate this model of aftershock occurrence. Many of the aftershocks locate within the mainshock rupture area, but generally in areas of relatively small slip at the edges of the slip concentrations. Note that the perimeter of the main shock rupture area would be the most strongly loaded by afterslip on a nearby compliant and weak-seismic areas. In general, however, the slip distributions plotted by Mendoza and Hartzell (1988) are spatially diffused by the inversion procedures: aftershocks on unruptured fault areas just outside or embedded inside the rupture area could appear to have occurred within the rupture area of the main shock.

6. The seismicity on the San Andreas fault at Parkfield and on the Calaveras fault

As a test of this frictional model, we consider the seismicity on faults where coseismic slip, aftershocks, and the interseismic seismicity are known. Our goal is to interpret the spatial and temporal features of the seismicity and slip during the coseismic, postseismic, and interseismic periods. Because of the availability of reliable earthquake locations and geodetic information, we consider the behavior of two strike-slip zones: the Parkfield segment of the San Andreas fault and the Morgan Hill and Coyote Lake segments of the southern Calaveras fault.

6.1. *The Parkfield segment of the San Andreas fault*

The Parkfield fault segment separates the central creeping section of the San Andreas from the locked Carrizo Plain section (fig. 7). Several moderate earthquakes ($M_L \leq 6.0$) have occurred on the Parkfield segment in the last 100 years, the most recent of which was on June 28, 1966. The Parkfield fault segment represents a unique opportunity to study a transitional region, that is, a fault area where a creeping zone and a seismogenic zone are close to each other along the strike direction.

The nomenclature of the «creeping section» of the San Andreas fault suggests that this region is characterized by a purely velocity-strengthening behavior while the transitional Parkfield section may contain both velocity-weakening and velocity-strengthening behavior. However, the seismicity shown in fig. 8a indicates that there is significant frictional heterogeneity within the creeping section. Earthquakes from 1970 to 1992 have been selected among those having rms errors less than 0.1 s, and at least 8 arrival times (Andy Michaels, written communication, 1993).

Many small earthquakes occur within the creeping section: the largest events have magnitudes close to 4. The seismic slip in these events is significantly less than the aseismic creep, however. Assuming a seismogenic

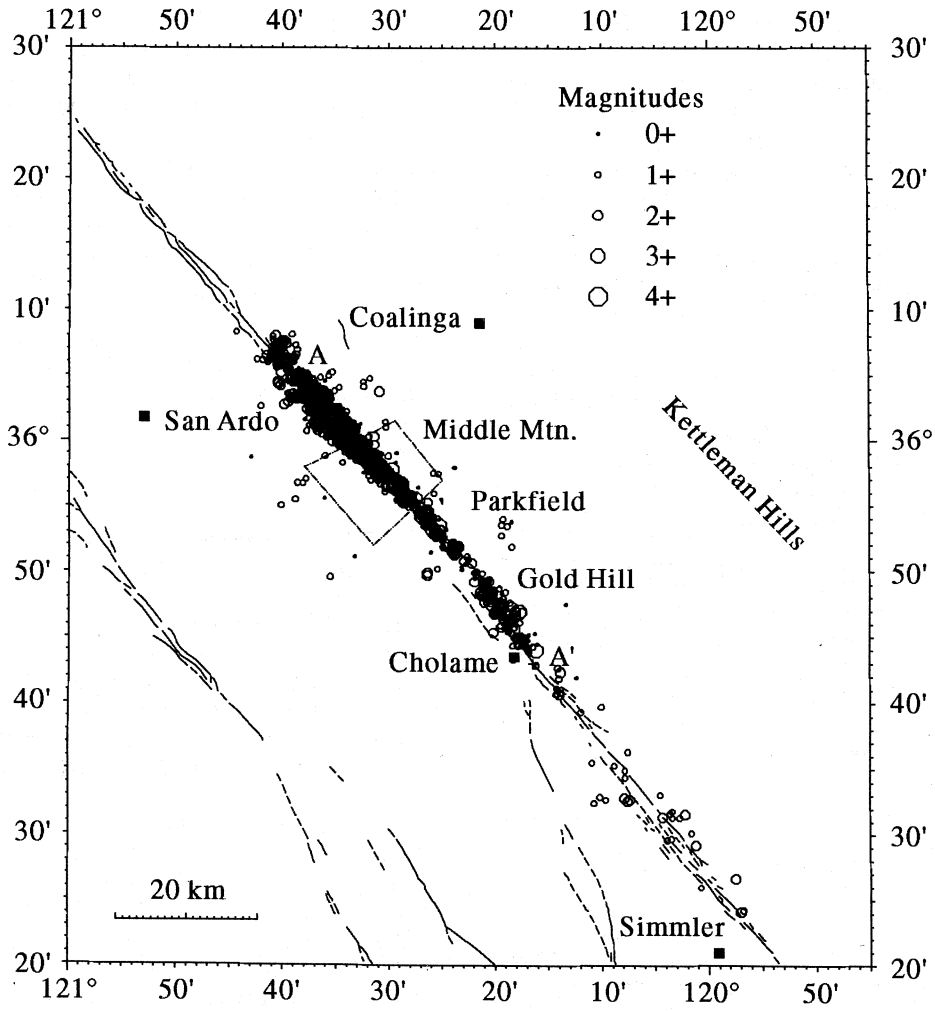

Fig. 7. Map of Parkfield seismicity from 1970 to 1992 from Michaels (written communication, 1993). The box represents the alert area for the Parkfield earthquake prediction experiment.

thickness of 7 km, the total seismic moment of 9.4×10^{24} dyne-cm released on the creeping section during the last 26 years (Oppenheimer, written communication, 1994) implies that the average seismic slip on the creeping section is $\approx$ 0.9 mm/year, or less than 3% of the 33 mm/year plate rate. The apparent density of earthquakes on the creeping section in fig. 8a is an artifact of the symbol sizes used for the events.

The occurrence of these interseismic events strongly suggests that velocity-weakening areas occur within the creeping section. We interpret this seismicity to indicate that the creeping section is a mosaic of fault areas that support small earthquakes and quasi-static slip,

respectively. The mixed frictional behavior of the creeping section could be obtained either through a heterogeneous distribution of $B - A$ with relatively small L's, or through $B \geq A$ with a heterogeneous distribution of L. The frequency-magnitude distribution of small earthquakes implies that L is distributed heterogeneously.

Figure 8b shows the distribution of aftershocks of the 1966 earthquake during the 6 months after the main shock. The absence of aftershocks within the creeping section is due to the selection criterion: there were few stations north of the 1966 epicenter after the earthquake. Comparison of fig. 8a,b yields a striking overlap between the distribution of the 1966 aftershocks and the interevent seismicity on the seismogenic section of the fault (Lindh, oral communication, 1984). We have lightly shaded the weak-seismic areas where the after-

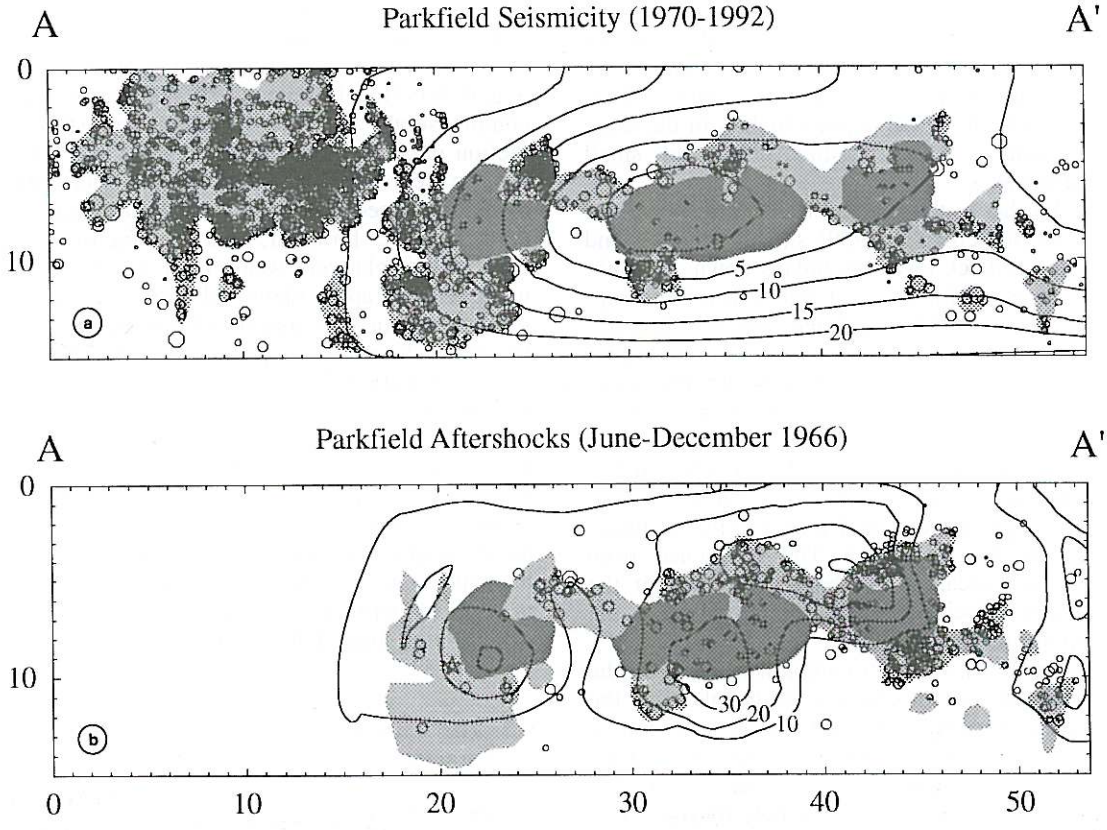

Fig. 8a,b. a) Cross-section of Parkfield seismicity from 1970 to 1992 located by Michaels (written communication, 1993), and the distribution of interseismic slip inferred by Harris and Segall (1986). b) Cross-section of the aftershocks occurring in the six months after the Parkfield earthquake, located by Michaels (written communication, 1993) using a minimum of 8 arrivals. The lack of earthquakes northwest of Middle Mountain reflects a lack of stations in this area. The light shading indicates the weak-seismic fault areas where the interseismic activity overlaps the aftershock activity. The contours show the distribution of coseismic slip in the 1966 earthquake obtained by Beroza (1989). The heavy shading indicates the inferred strong-seismic fault areas.

shocks and interseismic events overlap. All of the seismic area in the creeping section has been lightly shaded.

Figure 8b shows a comparison of the aftershock locations with the slip distribution obtained for the 1966 earthquake by Beroza (1989), who inverted the strong motion waveforms assuming a fixed rupture velocity of 0.75 β. Although the resolution of the slip is relatively weak, the aftershocks appear to be located at the edges of the slip concentrations. In particular, the cluster of aftershocks 4 km southeast and slightly updip of the hypocenter correlates with an (unslipped) reentrant in Beroza's (1989) slip distribution. Also, the slip concentration 12 km to the southeast of the epicenter appears bounded by a cluster of aftershocks at 11 km depth which is in the same location as a interseismic cluster of small earthquakes.

Further to the southeast, the correspondence between Beroza's (1989) slip distribution and the aftershock locations breaks down, as might be expected for an inversion with a fixed rupture velocity. The third and largest concentration of slip is 2-6 km deep and plots on top of the shallow band of aftershocks extending from 11 to 25 km southeast of the hypocenter. We interpret this contradiction with our model as a mislocation of the third subevent: judging from the aftershocks, the most likely area to have slipped is the shaded area to the southeast that is 4-8 km deep. The difference from Beroza's location can be accomodated if the rupture velocity increased above 0.75β as the rupture process evolved.

Figure 8a shows a comparison between the distribution of interseismic earthquakes and the interseismic slip inferred from an inversion of geodetic data by Harris and Segall (1987). Harris and Segall identify an area that is locked in the interseismic period. We note that this area is surrounded by both the interevent seismicity and the 1966 aftershocks, and roughly corresponds to the location of the second sub-event obtained by Beroza (1989). We have heavily shaded this area to indicate a strong-seismic region.

The resolution of Harris and Segall's (1987) inversion of geodetic data for interseismic slip is also weak, and the resulting image of the locked zone is conditioned by their smoothing constraints. The heavily shaded areas in fig. 8a,b indicate the fault areas that we interpret as strong-seismic, that is, fault areas that ruptured in the main shock and have remained locked during the subsequent interseismic period. The inferred slip of 5-15 cm on the shaded area near the 1966 hypocenter appears to contradict the frictional model. It is possible, however, that the geodetic data can be fit by assuming that the compliant and weak-seismic areas 5-8 km southeast of the 1966 hypocenter have slipped 5-15 cm instead of the 0-5 cm inferred by the inversion.

If these reinterpretations of the Harris and Segall (1987) and Beroza (1989) inversions are commensurate with the geodetic and strong motion data, then the crustal faulting at Parkfield is very well described by the frictional model proposed in this paper. Two observations suggest, however, that the faulting at Parkfield is relatively weak. First, none of the weak-seismic areas identified from the interseismic earthquakes appear to have ruptured in the main shock: that is, there are aftershocks wherever there is interseismic activity. In particular, the ligament between the second and third subevents, 20 km southeast of the hypocenter, has more aftershocks than would be driven by the reloading mechanism described in the preceding section. Second, there are small aftershocks distributed entirely across the rupture area of the second subevent rather than on its perimeter, as the reloading mechanism would suggest for a strong-seismic area.

6.2. *The Morgan Hill and Coyote Lake segments of the Calaveras fault*

Oppenheimer *et al.* (1990) investigated the occurrence of moderate-sized earthquakes and the distribution of interevent seismicity on the Calaveras fault (fig. 9) in order to consider the relative contribution of aseismic slip, seismic slip in frequent microearthquakes ($M \leq 3$), and episodic slip in moderate to large earthquakes. They considered three contiguous segments of the Calaveras fault, comparing the seismicity

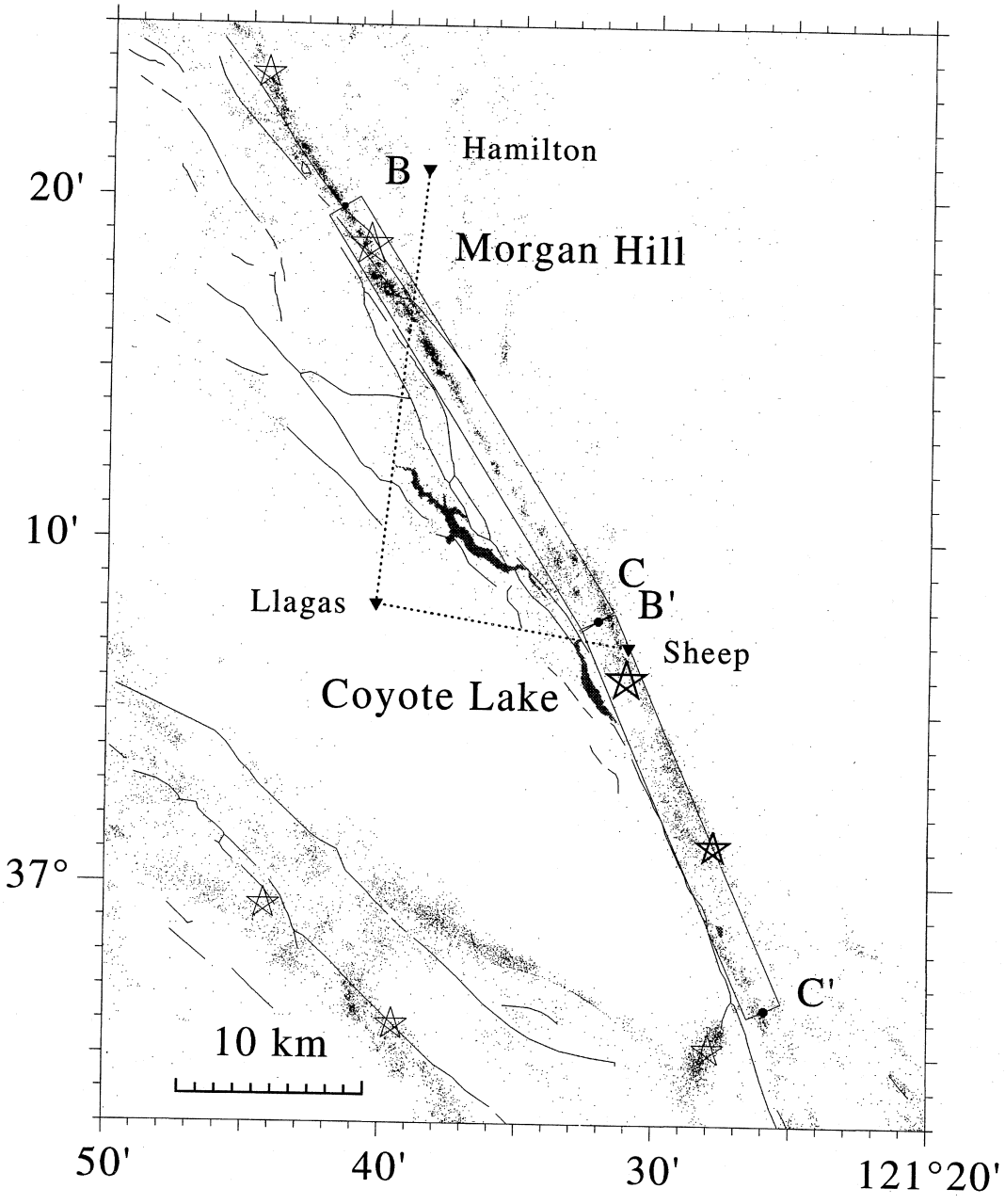

Fig. 9. Map of seismicity near the Calaveras fault provided by Oppenheimer (written communication, 1994). The tabular boxes contain the seismicity chosen for the following cross-sections: B-B′ for the Morgan Hill segment, and C-C′ for the Coyote Lake segment. The epicenters of the moderate earthquakes are indicated by stars. The inverted triangles show the geodetic stations at Mount Hamilton, Llagas Ranch, and Sheep Ranch.

before and after the 1979 Coyote Lake (M = 5.9), the 1984 Morgan Hill (M = 6.2), and the 1988 Alum Rock (M = 5.1) main shocks with the slip distributions obtained for the Morgan Hill earthquake by Hartzell and Heaton (1986), and for the Coyote Lake earthquake by Liu and Helmberger (1983).

Oppenheimer *et al.* (1990) concluded that fault areas with most of the interseismic activity do not generally slip during main shocks and must therefore slip aseismically. In contrast, they identified persistent patches that slip only during moderate earthquakes which are apparent as gaps in the interseismic activity extending from depth into the seismogenic sections of the fault. These areas correspond to the behaviors we described in the previous section as weak-seismic and strong-seismic. Oppenheimer *et al.* (1990) also proposed that similar gaps discerned from the interseismic earthquakes were candidate sites for future main shocks, and thereby predicted the location of a moderate earthquake (M = 5.2) that occurred in January 1993.

Figure 10 has been redrawn from the earthquakes plotted by Oppenheimer *et al.* (1990) in their cross sections of the seismicity on the Morgan Hill and Coyote Lake segments of the Calaveras fault. The time period spans the interval from 1969 to 1984. The upper cross sections show the distribution of seismicity before each main shock; the lower cross sections show six months of aftershocks following each main shock. The contour lines in the lower figures depict the slip distribution of the main shocks, taken from Beroza and Spudich (1988) for the Morgan Hill earthquake and from Liu and Helmberger (1983) for the Coyote Lake earthquake. The contour interval for the slip distributions is 25 cm; the stars indicate the mainshock hypocenters.

The slip distribution of Beroza and Spudich (1988) plots well below most of the aftershocks near the hypocenter. We interpret the northwestern part of the slip distribution to be mislocated 2 km in depth and 1 km southeast, so that the strong-seismic areas that failed in the main shock are situated on either side of the cluster of aftershocks 4 km southeast of the hypocenter. This relocates Beroza and Spudich's initial subevent to correspond with Hartzell and Heaton's (1986) first subevent. Also, the weak-seismic ligament between these two strong-seismic areas is interpreted to have ruptured in the main shock, as there are few aftershocks in this area.

As Oppenheimer *et al.* (1990) point out, the postseismic change in length of the Llagas-Hamilton geodetic line crossing the Morgan Hill fault (see fig. 9) was 1.8 times the coseismic change. The postseismic slip causing this length change was interpreted by Prescott *et al.* (1984) to occur at shallower depths than the seismic slip. The location of this line suggests that the observed postseismic slip occurred on and above the weak-seismic area above the northwestern part of the main shock rupture.

There is an extended aseismic area to the southwest of the second subevent, surrounding Beroza and Spudich's (1988) third subevent of the earthquake. The radiation from this subevent dominates the waveforms at many of the strong motion stations. We interpret the area surrounding the subevent to be compliant. Beroza and Spudich's location appears appropriate: the subevent area is surrounded by a cluster of aftershocks whose occurrence corresponds with the behavior expected of an abruptly loaded compliant area. Note that there were no interseismic earthquakes in this area. This area also slipped postseismically: the postseismic change of length of the Sheep-Llagas geodetic line is 1.5 times the coseismic change.

The lack of microseismicity could also be interpreted as indicating strong-seismic behavior. If part of this area is strong-seismic, however, it must fail within the seismic cycle. Oppenheimer *et al.* (1990) relocated the aftershocks of the ($M \approx 6.5$) 1911 earthquake near Morgan Hill and show that they span the same section of the Calaveras fault as the aftershocks of the 1984 earthquake. In contrast, there is no historic record of $5 \leq M \leq 6$ earthquakes on this aseismic section, whose occurrence would indicate a strong-seismic patch that fails on its own. Although such a short historic record can be misleading, it suggests that this extended aseismic area behaves compliantly.

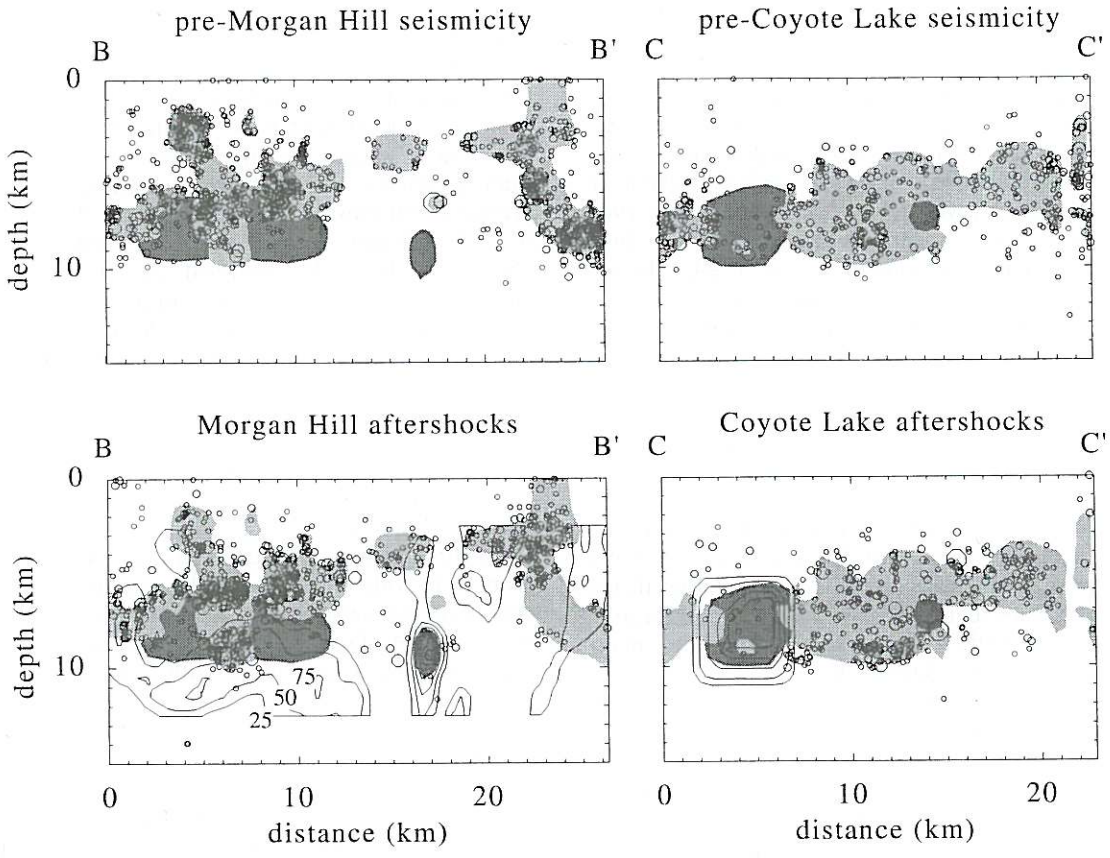

Fig. 10. Cross-sections of the seismicity on the Calaveras before the Morgan Hill and Coyote Lake earthquakes (right and left, respectively) as located by Oppenheimer (written communication, 1994), plotted above the seismicity on the Calaveras for the six months following each earthquake. The distribution of coseismic slip in the Morgan Hill earthquakes was obtained by Beroza and Spudich (1988), and for the Coyote Lake earthquake by Liu and Helmberger (1984). The light and heavy shading indicates the weak and strong-seismic fault areas, respectively.

The slip distribution obtained by Liu and Helmberger (1983) for the Coyote Lake earthquake fits within a 4 km wide gap in the interseismic activity. The northwestern part of the rupture contains a weak-seismic area where there was marked seismicity before the Coyote Lake earthquake. The extension of this weak-seismic area 4 km further to the northwest of the main shock rupture is anomalous, however, in that it has preseismic activity but did not slip in the main shock and had no aftershocks. It is possible that this area was ruptured by the subevents that occurred 6 and 12 s after the main shock, discerned in the teleseismic records by Nabelek (written communication, 1981). This stress release would have to have occurred relatively slowly as Liu and Helmberger (1983) could not identify the *S*-wave radiation from these subevents in the near-field accelegrams.

The heavily shaded area 11 km southeast of the Coyote Lake earthquake indicates the loca-

tion of the M = 5.2 earthquake that occurred January 14, 1993. This area was identified by Oppenheimer *et al.* (1990) as a likely source area for a moderate earthquake. There were very few aftershocks of this earthquake, despite its moderate size (Oppenheimer, oral communication, 1994). The previous event on this section was a M = 5.2 earthquake in 1949 that occurred near the epicenter of the 1993 earthquake (Oppenheimer *et al.* 1990). The unshaded area extending 5 km to the southeast of this event appears to behave compliantly.

There are two differences between the frictional interpretations of the seismicity on the Calaveras fault and the San Andreas fault at Parkfield. First, both the Morgan Hill and Coyote Lake main shocks appear to penetrate weak-seismic areas, although these interpretations require relocating part of Beroza and Spudich's (1988) slip distribution for the 1984 Morgan Hill earthquake and speculating that a slow subevent of the 1979 Coyote Lake earthquake ruptured to the northwest of the main shock rupture. Second, there is relatively more aseismic slip on the Calaveras fault than at Parkfield. Although the strong-seismic areas are situated at similar depths, on the Calaveras fault they are separated by extensive weak-seismic and compliant regions. Overall, it appears that as much as 80% of the Calaveras fault from 6 to 10 km depth creeps, either seismically or aseismically, during the interseismic period.

7. Discussion

We have articulated a frictional model for crustal faulting in which the variation between velocity-strengthening and velocity-weakening behavior controls the heterogeneity of moment release commonly observed in large earthquakes. Analyses of the interevent seismicity, coseismic slip, and aftershock distributions at Parkfield, Morgan Hill, and Coyote Lake appear to support this model of frictionally controlled faulting. In this section, we consider whether the fault geometry controls the frictional characteristics inferred for the Morgan Hill and Coyote Lake segments of the Calaveras fault.

Variations of the fault geometry lie outside the constraints of the purely planar model considered in the present paper. While many authors have written on the relations between fault geometry and fault segmentation, Andrews (1989) most eloquently describes the effect of a change in fault strike on fault mechanics. Andrews demonstrated that for vertical strike-slip faults, stress can only be transferred across a change in fault strike by introducing a secondary fault or branch fault to accomodate the out-of-plane motion. Because of the energy required for the associated volumetric deformation, Andrews (1989) argued that these «branch points» act as high-strength barriers that control the overall process of stress release on the fault.

At first glance, this geometric model appears to provide a critical insight into the variation between seismic and aseismic stress release on the Calaveras fault. If the strong-seismic areas can be associated with fault bends, or sections of the fault pinned between fault bends, then the planar fault sections might be frictionally weaker and could be assumed to creep.

The possibility of aseismic slip was not considered by Andrews (1989): we have introduced it here to accomodate Oppenheimer *et al.*'s (1990) inferences of interseismic creep. We test this hybrid model by comparing the fault geometry with the locations of the strong-seismic areas discerned from the slip distributions in the moderate and large earthquakes. Because the surface expression of these segments of the Calaveras fault is obscure, we will search the microseismic lineations in fig. 9 for variations of the fault geometry, assuming that the faults are purely vertical.

Starting with the Morgan Hill segment, then, we note a southwest inflection in the microseismicity 1-4 km southeast of the Morgan Hill epicenter which corresponds with the location of the initial subevent. It is difficult, however, to identify any other bends in the microseismicity, particularly in the section of the fault where the energetic third subevent is located. The deviation of 7° in strike between the

Morgan Hill and Coyote Lake segments occurs through an overlap of two subparallel lineations at the southeastern end of the Morgan Hill segment, rather than by branching near the main shock rupture area of the Coyote Lake earthquake. Finally, there is an offset in the lineation of microseismicity just to the southeast of the 1993 earthquake (Oppenheimer, oral communication, 1993).

Of the five strong-seismic areas identified on these two fault segments, then, only the first subevent of the Morgan Hill earthquake appears to be associated with a geometrical inflection, while there is a possible offset just southeast of the 1993 earthquake on the Coyote Lake segment. The other strong-seismic areas, in particular, the energetic third subevent of the Morgan Hill earthquake and the Coyote Lake main shock, occur on fault segments where the microseismicity appears linear. Although clearly not conclusive, this comparison fails to support the conjecture that the strong-seismic areas of the Calaveras fault are associated with fault bends.

8. Conclusions

In this paper, we differentiate velocity-weakening frictional behavior into strong and weak-seismic fields, and velocity-strengthening frictional behavior into compliant and viscous fields. The two limiting fields of this frictional classification, that is, the strong-seismic and the viscous fields, have been discussed at length by authors analyzing the effect of the depth dependence of friction on crustal faulting (Tse and Rice, 1986; Scholz, 1989; Rice, 1993).

The strong-seismic areas control the seismic cycle by releasing stress episodically in large earthquakes; in general, strong-seismic areas exhibit few aftershocks and little interseismic activity. The viscous areas sustain only stable sliding, in turn concentrating the tectonic load on the strong-seismic areas, and then accelerating or «rebounding» when they are loaded by the seismic failure of the strong-seismic areas.

We have proposed two intermediate fields of frictional behavior: the weak-seismic and the compliant fields. The behavior of these two fields is controlled by their proximity to the transition between velocity-weakening and velocity-strengthening. Weak-seismic areas can sustain dynamic instabilities during the coseismic and postseismic periods, but their interseismic behavior is determined by the slip weakening distance. In contrast, compliant areas creep aseismically during the interseismic period, but can be forced to dynamic instability by the abrupt application of a load, characteristically through the stress redistribution associated with a main shock. Thus, compliant areas can have aftershocks but not interseismic earthquakes.

If the critical slip weakening distance, L, is distributed heterogeneously so that $E[\Delta\tau/\delta] > (B-A)/\bar{L}$ for the compliance of an average patch of the fault, then a significant fraction of the weak-seismic fault area will creep aseismically while the remaining area fails in isolated small and moderate earthquakes. This process of «seismic creep» appears to correspond well with the frictional behavior observed for the most seismically active sections of the San Andreas and Calaveras faults, in particular, for the creeping section of San Andreas between San Juan Bautista and Parkfield. A similar interactive mechanism might underlie many earthquake swarms, in which the small and moderate earthquakes are loaded and reloaded by an ongoing creep event.

Observationally, these creeping weak-seismic areas appear to be resistant to dynamic rupture and may have acted as rupture «barriers» for the 1966 Parkfield earthquake (Aki, 1978). Similarly, compliant areas act as «absorbing barriers» that are resistant to dynamic rupture. In general, the larger the earthquake, the further the dynamic rupture will penetrate into the surrounding areas. Characteristically, large ($M \approx 7$) strike-slip earthquakes rupture coseismically to the surface while moderate ($M \approx 6$) strike-slip earthquakes are followed by prolonged surficial afterslip.

When a dynamic rupture decelerates in a compliant or creeping weak-seismic area, the rupture continues to grow quasi-statically, diffusing into a broad zone of accelerated afterslip and aftershocks. The most rapid afterslip occurs at the perimeter of the rupture area.

This rapid afterslip serves to reload areas of the fault that slipped in the main shock and then healed. If these areas are weak, but seismic, they can sustain secondary or «reloaded» aftershocks. We have modelled these aftershocks using spring-slider models with weak-seismic frictional characteristics. These reloaded aftershocks can be distinguished from aftershocks occurring through the delayed failure of isolated, unruptured fault areas by their relatively weak, or enervated, stress drops.

We have tested this frictional model of crustal faulting by examining the relationship of interseismic earthquakes, coseismic slip, and aftershocks for three moderate strike-slip earthquakes, the 1966 Parkfield, the 1979 Coyote Lake, and the 1984 Morgan Hill earthquakes. The faulting processes of these earthquakes appear well modelled by this frictional model, although this agreement requires relocating some of the coseismic slip distributions. It is unclear, however, if this frictional model can be applied as successfully to strike-slip faults with significantly lower strain rates than the San Andreas or the Calaveras faults.

Acknowledgements

We thank the International School of Geophysics for the opportunity to present this work at Erice. We are greatly indebted to Marie-Elina Belardinelli and Dave Oppenheimer for many discussions that helped us to articulate and test these hypotheses. Conversations with Maurizio Bonafede, Paul Okubo, Jim Dieterich, Andy Michaels, Claudio Chiarabba, Jim Rice, and Enzo Boschi greatly improved our understanding of fault processes. We thank Joe Andrews and Paul Spudich for their prompt reviews of this paper. J.B. was supported by a Gilbert Fellowship from the U.S. Geological Survey, and worked as a visiting researcher at the Istituto Nazionale di Geofisica while in residence at the American Academy in Rome. The support of each of these institutes is gratefully acknowledged. This paper is abbreviated from Boatwright and Cocco (1995) that will be published in the *Journal of Geophysical Research.*

REFERENCES

AKI, K. (1978): Characterization of barriers on an earthquake fault, *J. Geophys. Res.*, **84**, 6140-6148.

ANDREWS, D.J. (1989): The mechanics of fault junctions, *J. Geophys. Res.*, **94**, 9389-9397.

BEROZA, G. (1989): *PhD Thesis*, MIT, Cambridge MA.

BEROZA, G. and P. SPUDICH (1988): Linearized inversion for fault rupture behavior: application to the 1984 Morgan Hill, California, earthquake, *J. Geophys. Res.*, **93**, 6275-6296.

DAS, S. and B. KOSTROV (1983): Breaking of a single asperity: rupture process and seismic radiation, *J. Geophys. Res.*, **88**, 4277-4288.

DIETERICH, J.H. (1972): Time dependent friction as a possible mechanism for aftershocks, *J. Geophys. Res.*, **77**, 3771-3781.

DIETERICH, J.H. (1978): Time dependent friction and the mechanics of stick slip, *Pure and Appl. Geophys.*, **116**, 790-806.

DIETERICH, J.H. (1979a): Modeling of rock friction, I, experimental results and constitutive equations, *J. Geophys. Res.*, **84**, 2161-2168.

DIETERICH, J.H. (1979b): Modeling of rock friction, II, simulation of preseismic slip, *J. Geophys. Res.*, **84**, 2169-2175.

DIETERICH, J.H. (1980): Experimental and model study of fault constitutive properties, in *Solid Earth Geophysics and Geotechnology*, edited by S. NEMAT-NASSER, AMD **42**, 21-29, American Society of Mechanical Engineers.

DIETERICH, J.H. (1981): Constitutive properties of faults with simulated gouge, in *Mechanical Behavior of Crustal Rocks*, edited by N. I. CARTER, M. FRIEDMAN, J. M. LOGAN and D.W. STEARNS, *Geophys. Monogr. Ser.*, **24**, 103-120, AGU, Washington D.C.

DIETERICH, J.H. (1986): A model for the nucleation of earthquake slip, in *Earthquake Source Mechanics*, edited by S. DAS, J. BOATWRIGHT and C.H. SCHOLZ, Am. Geophys. Union, Geophys. Monogr. 37, Washington, D.C., *Maurice Ewing Series*, **6**, 37-47.

GU, J.C., J.R. RICE, A.L. RUINA, and S.T. TSE (1984): Slip motion and stability of a single degree of freedom elastic system with rate and state dependent friction, *J. Mech. Phys. Solids*, **32**, 167-196.

HARRIS, R.A. and P. SEGALL (1987): Detection of a locked zone at depth on the Parkfield, California, segment of the San Andreas fault, *J. Geophys. Res.*, **92**, 7945-7962.

HARTZELL, S.H. and T.H. HEATON (1986): Rupture history of the 1984 Morgan Hill, California, earthquake from the inversion of ground motion records, *Bull. Seismol. Soc. Am.*, **76**, 649-674.

KANAMORI, H. (1981): The nature of seismicity patterns before large earthquakes, in *Earthquake Prediction – An International Rewiev*, edited by D. SIMPSON and P.G. RICHARDS, AGU, Washington, D.C., *Maurice Ewing Series*, **4**, 1-19.

KING, G.C.P. (1986): Speculations on the geometry of the initiation and termination of earthquake rupture and its relation to morphology and geological structure, *Pure and Appl. Geophys.*, **124**, 567-585.

LACHENBRUCH, A. and J. SASS (1973): Thermo-mechanical

aspects of the San Andreas, in *Proceedings Conference on the Tectonic Problems of the San Andreas Fault System*, edited by R.K. KOVACH and A. NUR, Stanford University Press, Palo Alto, California, *Publ. Geol. Science*, **13**, 192-205.

LIU, H. and D. V. HELMBERGER (1983): The near source ground motion of the August 6, 1979 Coyote Lake, California, earthquake, *Bull. Seismol. Soc. Am.*, **73**, 201-218.

MARONE, C., C.B. RALEIGH and C.H. SCHOLZ (1990): Frictional behavior and constitutive modeling of simulated fault gouge, *J. Geophys. Res.*, **95**, 7007-7025.

MARONE, C., C.H. SCHOLZ and R. BILHAM (1991): On the mechanics of earthquake afterslip, *J. Geophys. Res.*, **96**, 8441-8452.

MENDOZA, C. and S.H. HARTZELL (1988): Aftershocks patterns and mainshock faulting, *Bull. Seismol. Soc. Am.*, **78**, 1438-1449.

MIKUMO, T. (1992): Dynamic fault rupture and stress recovery processes in continental crust under depth-dependent shear strength and frictional parameters, *Tectonophysics*, **211**, 201-222.

MIYATAKE, T. (1992): Numerical simulation of three-dimensional faulting processes with heterogeneous rate- and state-dependent friction, *Tectonophysics*, **211**, 223-232.

OKUBO, P.G. (1989): Dynamic rupture modeling with laboratory derived constitutive relations, *J. Geophys. Res.*, **94**, 12321-12336.

OKUBO, P.G. and J.H. DIETERICH (1986): State variable fault constitutive relations for dynamic slip, in *Earthquake Source Mechanics*, edited by S. DAS, J. BOATWRIGHT, and C. SCHOLZ, *AGU Geophys. Monogr.*, **37**, 25-35, American Geophys. Union.

OPPENHEIMER, D.H., W.H. BAKUN and A.G. LINDH (1990): Slip partitioning of the Calaveras fault, California, and prospects for future earthquakes, *J. Geophys. Res.*, **95** B6, 8483-8498.

PRESCOTT, W.H., N.E. KING and G. GUOHUA (1984): Preseismic, coseismic, and postseismic deformation associated with the 1984 Morgan Hill, California, earthquake, the 1984 Morgan Hill, California, Earthquake, Calif. Depth. of Conserv., Division of Mines and Geology, Sacramento, *Spec. Publ.*, n. 68, 137-148.

PRESS, W.H., B.P. FLANNERY, S.A. TEUKOLSKY and W.T. VETTERLING (1979): *Numerical Recipes* (Cambridge University Press, 1989).

QUIN, H. (1990): Dynamic stress drop and rupture dynamics of the October 15, 1979, Imperial Valley, California, earthquake, *Tectonophysics*, **175**, 93-118.

RICE, J.R. (1993): Spatio-temporal complexity of slip on a fault, *J. Geophys. Res.*, **98** (B6), 9885-9907.

RICE, J.R. and A.L. RUINA (1983): Stability of steady frictional slipping, *J. Appl. Mech.*, **50**, 343-349.

RICE, J.R. and J. GU (1983): Earthquake aftereffects and triggered seismic phenomena, *Pure and Appl. Geophys.*, **121**, 187-219.

RICE, J.R. and S.T. TSE (1986): Dynamic motion of a single degree of freedom system following a rate and state dependent friction law, *J. Geophys. Res.*, **91**, 521-530.

RUINA, A.L. (1980): Friction laws and instabilities: a quasi-static analysis of some dry friction behavior, *Ph.D. Thesis*, Brown University, Providence, R.I.

RUINA, A.L. (1983): Slip instability and state variable friction laws, *J. Geophys. Res.*, **88**, 10359-10370.

SCHOLZ, C.H. (1988): The brittle-plastic transition and the depth of seismic faulting, *Geol. Runds.*, **77**, 319-328.

SCHOLZ, C.H. (1989): Mechanics of faulting, *Am. Rev. Planet. Sci.*, **17**, 309-334.

SCHOLZ, C.H. (1990): *The Mechanics of Earthquakes and Faulting* (Cambridge University Press), pp. 433.

SIBSON, R.H. (1984): Roughness at the base of the seismogenic zone: contributing factors, *J. Geophys. Res.*, **89**, 5791-5799.

SIBSON, R.H. (1986): Rupture interaction with fault jogs, in *Earthquake Source Mechanics*, edited by S. DAS, J. BOATWRIGHT and C. SCHOLZ, American Geophys. Union, *AGU Geophys. Monogr.*, **37**, 157-168.

TSE, S.T., R. DMOWSKA and J. R. RICE (1985): Stressing of locked patches along a creeping fault, *Bull. Seismol. Soc. Am.*, **75**, 709-736.

TSE, S.T. and J. R. RICE (1986): Crustal earthquake instability in relation to the depth variation of frictional slip properties, *J. Geophys. Res.*, **91**, 9452-9472.

WESSON, R.L. (1987): Modelling aftershock migration and aftership of the San Juan Bautista earthquake of October 3, 1972, *Tectonophysics*, **144**, 215-229.